

UCLA

UCLA Previously Published Works

Title

Precision Radiotherapy: Reduction in Radiation for Oropharyngeal Cancer in the 30 ROC Trial

Permalink

<https://escholarship.org/uc/item/9rh8q0mq>

Journal

Journal of the National Cancer Institute, 113(6)

ISSN

0027-8874

Authors

Riaz, Nadeem
Sherman, Eric
Pei, Xin
et al.

Publication Date














2021-06-01

DOI

10.1093/jnci/djaa184

Peer reviewed

Precision Radiotherapy: Reduction in Radiation for Oropharyngeal Cancer in the 30 ROG Trial

Nadeem Riaz, MD,^{1,2,‡} Eric Sherman, MD,^{3,‡} Xin Pei , PhD,^{1,‡} Heiko Schöder, MD,⁴ Milan Grkovski , PhD,⁵ Ramesh Paudyal , PhD,⁵ Nora Katabi, MD,⁶ Pier Selenica, BSc,⁶ Takafumi N. Yamaguchi , PhD,^{7,8,9} Daniel Ma , MD,¹⁰ Simon K. Lee, MSc,⁶ Rachna Shah , BSc,¹ Rahul Kumar , PhD,¹¹ Fengshen Kuo , PhD,² Abhirami Ratnakumar , PhD,¹ Nathan Aleynick, BSc,⁶ David Brown, PhD,¹¹ Zhigang Zhang, PhD,¹² Vaios Hatzoglou, MD,⁴ Lydia Y. Liu, PhD,^{7,8,9,13,14} Adriana Salcedo, PhD,^{8,13} Chiaojung J. Tsai , MD,¹ Sean McBride, MD,¹ Luc G. T. Morris , MD,^{2,15} Jay Boyle, MD,¹⁵ Bhuvanesh Singh, MD, PhD,¹⁵ Daniel S. Higginson , MD,¹ Rama R. Damerla, PhD,¹ Arnaud da Cruz Paula, BSc,⁶ Katharine Price, MD,¹⁶ Eric J. Moore , MD,¹⁷ Joaquin J. Garcia, MD,¹⁸ Robert Foote , MD,¹⁰ Alan Ho, MD, PhD,³ Richard J. Wong, MD,¹⁵ Timothy A. Chan, MD, PhD,^{1,2,19} Simon N. Powell, MD, PhD,¹ Paul C. Boutros , PhD,^{7,8,9,13,20,21,22} John L. Humm, PhD,⁵ Amita Shukla-Dave, PhD,^{4,5} David Pfister, MD,³ Jorge S. Reis-Filho, MD, PhD,^{6,19,*} Nancy Lee, MD^{1,*}

¹Department of Radiation Oncology, Memorial Sloan Kettering Cancer Center, New York, NY, USA; ²Immunogenomics and Precision Oncology Platform, Memorial Sloan Kettering Cancer Center, New York, NY, USA; ³Department of Medical Oncology, Memorial Sloan Kettering Cancer Center, New York, NY, USA; ⁴Department of Radiology, Memorial Sloan Kettering Cancer Center, New York, NY, USA; ⁵Department of Medical Physics, Memorial Sloan Kettering Cancer Center, New York, NY, USA; ⁶Department of Pathology, Memorial Sloan Kettering Cancer Center, New York, NY, USA; ⁷UCLA, Department of Human Genetics, Los Angeles, CA, USA; ⁸Informatics and Biocomputing Program, Ontario Institute for Cancer Research, Toronto, ON, USA; ⁹Jonsson Comprehensive Cancer Centre, University of California, Los Angeles, CA, USA; ¹⁰Department of Radiation Oncology, Mayo Clinic, Rochester, MN, USA; ¹¹Institute for Cancer Genetics, Columbia University, New York, NY, USA; ¹²Department of Biostatistics, Memorial Sloan Kettering Cancer Center, New York, NY, USA; ¹³Department of Medical Biophysics, University of Toronto, Toronto, ON, USA; ¹⁴Vector Institute for Artificial Intelligence, Toronto, ON, USA; ¹⁵Department of Surgery, Memorial Sloan Kettering Cancer Center, New York, NY, USA; ¹⁶Division of Medical Oncology, Mayo Clinic, Rochester, MN, USA; ¹⁷Department of Otolaryngology, Mayo Clinic, Rochester, MN, USA; ¹⁸Department of Pathology, Mayo Clinic, Rochester, MN, USA; ¹⁹Human Oncology and Pathogenesis Program, Memorial Sloan Kettering Cancer Center, New York, NY, USA; ²⁰Department of Pharmacology and Toxicology, University of Toronto, Toronto, ON, USA; ²¹Department of Urology, University of California, Los Angeles, CA, USA and ²²Institute for Precision Health, University of California, Los Angeles, CA, USA

‡Authors contributed equally to this work.

*Correspondence to: Nancy Lee, MD, Memorial Sloan Kettering Cancer Center, 1275 York Ave, New York, NY 10065, USA (e-mail: leen2@mskcc.org) and Jorge S. Reis-Filho, MD, PhD, 1275 York Ave, New York, NY 10065, USA (e-mail: reisfilj@mskcc.org).

Abstract

Background: Patients with human papillomavirus-related oropharyngeal cancers have excellent outcomes but experience clinically significant toxicities when treated with standard chemoradiotherapy (70 Gy). We hypothesized that functional imaging could identify patients who could be safely deescalated to 30 Gy of radiotherapy. **Methods:** In 19 patients, pre- and intratreatment dynamic fluorine-18-labeled fluoromisonidazole positron emission tomography (PET) was used to assess tumor hypoxia. Patients without hypoxia at baseline or intratreatment received 30 Gy; patients with persistent hypoxia received 70 Gy. Neck dissection was performed at 4 months in deescalated patients to assess pathologic response. Magnetic resonance imaging (weekly), circulating plasma cell-free DNA, RNA-sequencing, and whole-genome sequencing (WGS) were performed to identify potential molecular determinants of response. Samples from an independent prospective study were obtained to reproduce molecular findings. All statistical tests were 2-sided. **Results:** Fifteen of 19 patients had no hypoxia on baseline PET or resolution on intratreatment PET and were deescalated to 30 Gy. Of these 15 patients, 11 had a pathologic complete response. Two-year locoregional control and overall survival were 94.4% (95% confidence interval = 84.4% to 100%) and 94.7% (95% confidence interval = 85.2% to 100%), respectively. No acute grade 3 radiation-related toxicities were observed.

Received: July 14, 2020; Revised: August 21, 2020; Accepted: October 2, 2020

© The Author(s) 2021. Published by Oxford University Press. All rights reserved. For permissions, please email: journals.permissions@oup.com

Microenvironmental features on serial imaging correlated better with pathologic response than tumor burden metrics or circulating plasma cell-free DNA. A WGS-based DNA repair defect was associated with response ($P = .02$) and was reproduced in an independent cohort ($P = .03$). **Conclusions:** Deescalation of radiotherapy to 30 Gy on the basis of intratreatment hypoxia imaging was feasible, safe, and associated with minimal toxicity. A DNA repair defect identified by WGS was predictive of response. Intratherapy personalization of chemoradiotherapy may facilitate marked deescalation of radiotherapy.

Human papillomavirus (HPV)-related oropharyngeal cancers (OPCs) have molecular features and etiology distinct from those of smoking- and alcohol-related head and neck cancers (HNCs) (1-3). Concurrent cisplatin chemotherapy and 70 Gy of radiation is the mainstay of treatment for patients with HPV-related OPCs and results in excellent outcomes (4,5). Preclinical and clinical studies demonstrate that these tumors are exquisitely sensitive to chemoradiotherapy, with most patients cured of disease (5-7). Many patients, though cured, suffer from clinically significant acute and late treatment-related toxicities (8,9). Current deescalation approaches include modest reduction of the radiation dose in chemoradiotherapy (10), replacement of cisplatin with an alternative systemic therapy (11,12), elimination of chemotherapy or reduction of the radiation dose after trans-oral robotic surgery (13,14), and use of the response to induction chemotherapy to guide radiation dose and tumor target volume (15-17). Unfortunately, the radiation deescalation pursued in many of these studies is modest, given the general concerns about its detrimental impact on patient outcome, and has not resulted in a statistically significant reduction in toxicity (11,12).

HPV is known to deregulate the DNA damage response (DDR), which has been posited to mediate the radiosensitivity of HPV-related cancers (6,18-22). Amplification of the HPV viral genome often results in aberrant DNA structures, which leads to a dysregulated response from the DDR machinery (23,24). Further, E7 directly interacts with members of the DDR and decreases the efficacy of double-strand break (DSB) repair by nonhomologous end-joining (22,25). Consistent with this notion, in other HPV-related malignancies, such as anal cancer, 30 Gy and chemotherapy can result in a 95% rate of cure (26). Additionally, tumor hypoxia has been known to mediate radiation resistance (27), resulting in poor outcomes in multiple malignancies, including HPV-related OPCs (28-30). We have demonstrated that tumor hypoxia can be robustly measured in HNCs with fluorine-18-labeled fluoromisonidazole positron emission tomography (^{18}F -FMISO PET) (31,32). We also previously reported the feasibility of hypoxia assessment using functional imaging with ^{18}F -FMISO PET for HPV-related OPC patients undergoing chemoradiation, and successfully deescalated radiation dose to 60 Gy for those whose tumors did not demonstrate hypoxia (31,32).

Here, we report on an expansion cohort that investigates the feasibility of using hypoxia imaging to identify patients with radiosensitive OPC who may be able to receive a nearly 60% lower dose of radiotherapy from a standard dose of 70 Gy to a deescalated dose of 30 Gy. We hypothesized that 30 Gy of chemoradiotherapy delivered before neck dissection would lead to a high rate of pathologic complete response (pCR) in patients who lacked radiological features of tumor hypoxia at diagnosis or during treatment. Further, to derive new biologic premises to guide future deescalation efforts, we performed hypothesis-generating analyses based on whole-genome and transcriptome sequencing as well as longitudinal functional imaging analysis. The results of these analyses were further tested in an independent prospective cohort of HPV-related OPC patients receiving low-dose adjuvant radiotherapy with concurrent chemotherapy.

Methods

Trial Design

Patients with T1-2, N1-2b (American Joint Committee on Cancer Staging Manual, 7th edition) (33), p16-positive ($\geq 70\%$ nuclear and cytoplasmic staining; Ventana Medical Systems) tumors of the tonsil, base of tongue, glossotonsillar sulcus, or an unknown primary were prospectively enrolled on an expansion cohort from July 2015 to October 2016 (ClinicalTrials.gov number NCT00606294; Cohort 2) at Memorial Sloan Kettering Cancer Center (MSK). All patients were discussed at our multidisciplinary OPC conference before enrollment on our institutional review board-approved protocol. Patient consent was obtained for every patient. Eligible patients were candidates for platin-based chemotherapy with a primary tumor deemed to be resectable.

Patients first underwent resection of the primary tumor (Supplementary Figure 1, available online). Neither robotic surgery nor obtaining a negative margin was mandatory. Ipsilateral tonsillectomy and a core biopsy of a cervical lymph node were required for unknown primary tumors. Two to 4 weeks after surgery, patients underwent fluorodeoxyglucose PET or computed tomography-based simulation for radiation planning. This was followed by a ^{18}F -FMISO PET to evaluate pretreatment hypoxia status of lymphatic disease in all patients.

Patients with pretreatment hypoxia on ^{18}F -FMISO PET underwent a repeat intratreatment ^{18}F -FMISO PET 5 to 10 days after the start of chemoradiotherapy. Patients without pretreatment hypoxia or patients with intratreatment resolution of hypoxia on intratreatment imaging received 30 Gy in 15 daily fractions to gross nodal disease, postoperative tumor bed, and all microscopic regions deemed to be at risk, with 2 cycles of cisplatin at 100 mg/m^2 . For noncisplatin patients, carboplatin with an area under the curve of 1.25 intravenously daily $\times 4$ days (total dose of area under the curve of 5) and 5-Fluorouracil at a dose of 600 mg/m^2 intravenous infusion (total of 2400 mg/m^2 intravenous infusion over 96 hours) were given on days 1 and 22 (34). Chemotherapy dose reductions were not permitted for patients receiving 30 Gy. Patients with evidence of persistent hypoxia on intratreatment ^{18}F -FMISO PET were treated to 70 Gy (Supplementary Figure 1, available online).

Patients were assessed monthly until 3 to 4 months after the end of chemoradiotherapy; at this time, a fluorodeoxyglucose PET or computed tomography was obtained to assess response, followed by a mandatory selective neck dissection to ensure pathologic eradication of disease. Histologic assessment of neck dissection specimens was made by the study pathologist (N.K.), and response (fibrosis, necrosis, inflammation) was quantified for cases with residual disease. Patients were subsequently followed every 3 to 4 months thereafter.

Assessment of Tumor Hypoxia by ^{18}F -FMISO PET Imaging

Absence of pretreatment hypoxia or intratreatment resolution of hypoxia was deemed to indicate radiosensitivity and

qualified a patient for deescalation (31). Dynamic PET acquisition for a 15-cm field of view started simultaneously with the intravenous bolus injection of ^{18}F -FMISO (8-10 mCi). These initial dynamic images were obtained for a total of 30 minutes (31). The last 15 minutes were summed into 1 static image for review. Additional static images were obtained approximately 150 minutes after injection of radiotracer. Determination of the presence or absence of hypoxia was made on the basis of visual inspection and in accordance with the well-established tumor-muscle activity ratio (>1.2) on the late static ^{18}F -FMISO PET image by 1 nuclear medicine physician (H.S.) (19). Dynamic scans were used to perform compartmental analysis (Supplementary Methods, available online) (35).

Magnetic Resonance Imaging (MRI)

MRI examinations were performed on a Philips 3 T MRI scanner (Ingenia, Philips Healthcare, the Netherlands) using a neurovascular phased array. Images were obtained pretreatment, weekly during therapy, and at 1, 2, 3, and 4 months after radiotherapy. Diffusion-weighted images and dynamic contrast enhanced-MRI imaging were also obtained (Supplementary Methods, available online).

Statistical Analysis

Using the decision rule that at least 10 patients are alive with follow-up and have a pCR at 4 months after chemoradiotherapy, we estimated that 14 eligible patients for deescalation would be deemed feasible for further study (Supplementary Methods, available online). To account for attrition, we assumed approximately 25% of the enrolled patients would not undergo deescalation. Therefore, we recruited 19 patients up front but counted only the first 14 patients toward the decision rule. Data for all analysis were locked on September 17, 2019.

Genomic Analysis

Tumors were harvested in fresh RPMI 1640 media after primary resection and was immediately embedded in optimal cutting temperature compound and stored at -80°C . Each histologic specimen was reviewed by a board-certified pathologist (N.K.). To obtain high-purity tumor, specimens were microdissected under a stereo microscope before DNA and RNA extraction as previously described (36). In cases where insufficient material was obtained from frozen specimens, formalin-fixed, paraffin-embedded specimens were used instead. Mutation detection was conducted using our validated pipeline (Supplementary Methods, available online) (36). RNA sequencing was performed using the transcriptome capture process on an Illumina TruSeq RNA kit in accordance with the manufacturer's protocol (Supplementary Methods, available online). Circulating plasma cell-free HPV-DNA assessment was also performed pre-, intra-, and posttherapy by digital droplet PCR (Supplementary Methods, available online).

Independent Cohort for the Testing of Correlative Findings

We obtained a set of 19 cases from a Mayo Clinic study (ClinicalTrials.gov identifier, NCT01932697) of low-dose adjuvant radiotherapy to 30 Gy with concurrent docetaxel as an

independent cohort for the testing of the genomic findings stemming from the analysis of the patients from NCT00606294 (13,36). Nine of these patients developed recurrence (either locoregional or distant) and 10 are disease free (Supplementary Methods, available online).

Results

Patients

Nineteen patients were enrolled (Table 1). All patients underwent resection of their primary tumor, with a median size of 1.75 cm (range = 0.7-2.7 cm; Supplementary Table 1, available online). Two of 3 patients with unknown primary tumors underwent bilateral tonsillectomies, and 1 underwent an ipsilateral tonsillectomy. The median time between surgery and start of radiotherapy was 4.8 weeks (range = 3.1-12.7 weeks). Pretreatment ^{18}F -FMISO PET scans (n = 19) were obtained at a median of 1.4 weeks (range = 0-2.86 weeks) before the initiation of chemoradiotherapy. Of these 19 pretreatment ^{18}F -FMISO PET scans, 6 lacked imaging features of hypoxia, whereas 13 displayed pretreatment hypoxia (Figure 1). One patient with a positive pretreatment ^{18}F -FMISO PET developed an intercurrent illness with prolonged hospitalization unrelated to his cancer or treatment; this patient was removed from the study and received standard treatment with 70 Gy of radiotherapy with chemotherapy. For the remaining 12 patients with positive pretreatment ^{18}F -FMISO PETs, a repeat ^{18}F -FMISO PET scan was performed to assess early response to chemoradiotherapy at a median of the 10th radiation fraction (range = sixth to 10th fraction). Of these patients, 9 had resolution of hypoxia. Together with the 6 patients without pretreatment hypoxia, a total of 15 patients were deescalated to 30 Gy (Figure 1; Supplementary Figures 2 and 3, available online). One of the 15 deescalated

Table 1. Patient characteristics (n = 19)^a

Characteristic	No. (%)
Sex	
Male	16 (84.2)
Female	3 (15.8)
Age, median (range), y	57 (44-70)
Smoking	
Never	11 (57.9)
<10 pack-years	6 (31.6)
>10 pack-years	2 (10.5)
Primary site	
Tonsil	11 (57.9)
Base of tongue	5 (26.3)
Unknown primary	3 (15.8)
T class	
1	11 (57.9)
2	5 (26.3)
X	3 (15.8)
N class	
1	5 (26.3)
2a	3 (15.8)
2b	11 (57.9)
Stage	
III	5 (26.3)
IVa	14 (73.7)

^aClinical, Demographic, and American Joint Committee on Cancer 7th edition staging characteristics of patients enrolled in the study.

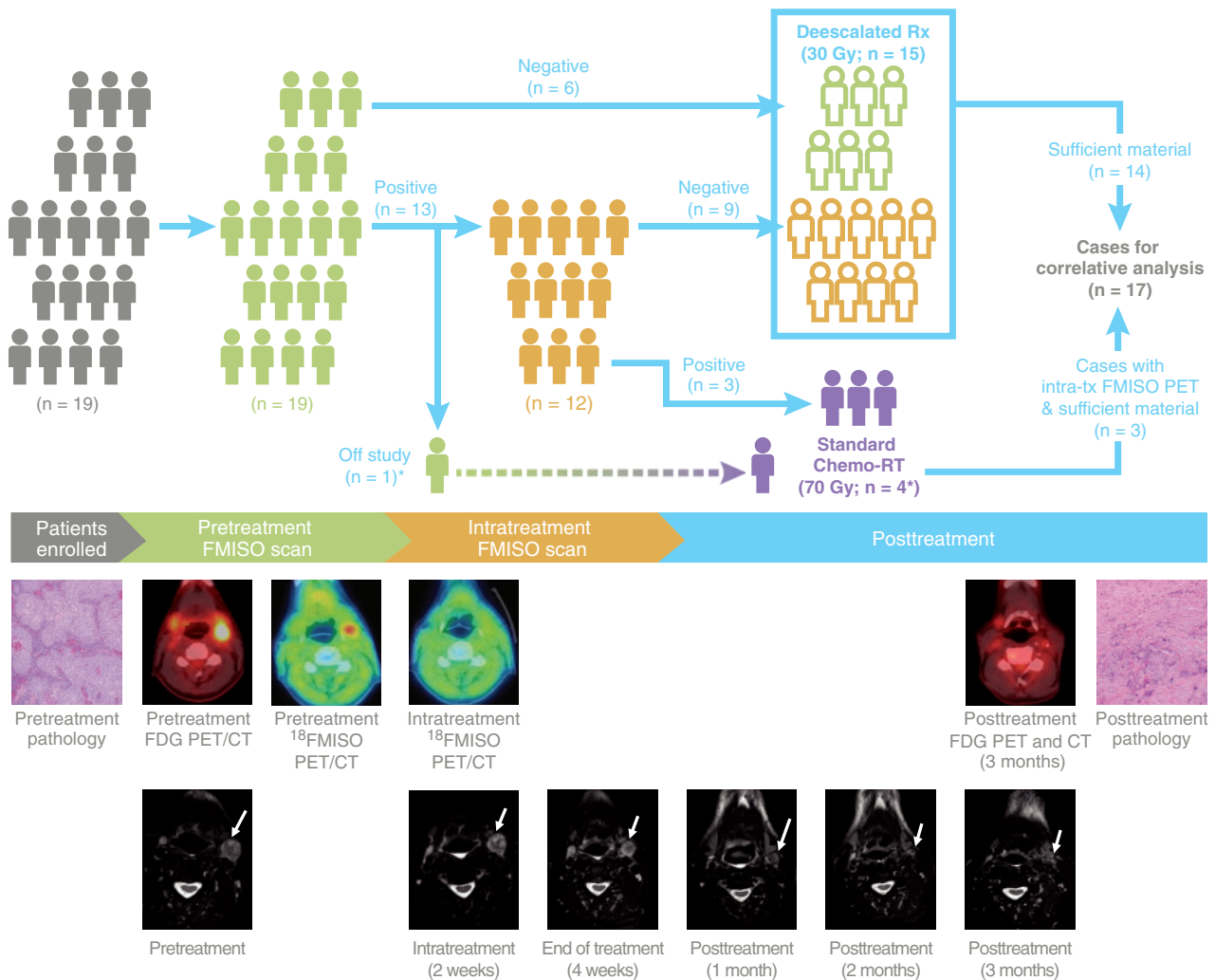


Figure 1. Precision radiotherapy (RT) and longitudinal imaging. **Top**) Study schema and results of pre- and intratreatment fluorine-18-labeled fluoromisonidazole positron emission tomography (^{18}F -FMISO PET) scans (see also [Supplementary Figure 1](#), available online). One patient was removed from the study before his intratreatment scan because of an unrelated medical illness and received the standard 70 Gy of chemo-RT. **Bottom**) In the illustrated case, intratreatment hypoxia resolved after the 10th fraction of treatment. Intratreatment ^{18}F -FMISO PET demonstrates resolution of hypoxia. Weekly on-therapy and monthly posttreatment monitoring of therapy with T2-weighted magnetic resonance imaging was performed. Increasing T2-hyperintensity during therapy is consistent with solid tumor turning into fluid, although the anatomic size of the gross nodal disease did not decrease. Posttherapy, the involved lymph node slowly regressed (selected images shown). Posttreatment PET and computed tomography (CT) demonstrated resolution of FDG avid disease, and subsequent neck dissection demonstrated complete pathologic response. *Note, one patient was removed from study due before his intra-treatment scan due to an unrelated medical illness, and was analyzed in standard 70Gy Chemo-rt group.

patients had a clinically significant protocol deviation (receipt of only 1 cycle of cisplatin).

Pathologic and Clinical Outcomes

Median follow-up was 34 months (range = 18-41 months). Eleven of the 15 patients who received 30 Gy had a pCR on posttreatment neck dissection ([Figure 2A](#)). Of the 4 patients with residual disease, only 1 treated per protocol had clearly clinically significant residual disease; notably, this patient developed rapid tumor regrowth shortly after treatment as detected by monthly posttreatment MRI ([Supplementary Figure 4](#), available online). Two patients with residual disease had minimal foci of uncertain viability ([Supplementary Figure 4](#), available online) and did not receive any further treatment. The sole patient deescalated who deviated from the protocol developed

progressive locoregional disease. Of the 2 patients with longer than a 10 pack-year smoking history, neither of whom was an active smoker, 1 patient had minimal residual disease at neck dissection ([Supplementary Table 1](#), available online). Two-year locoregional control, progression-free survival, and overall survival for the deescalated cohort per protocol were 100% (95% confidence interval [CI] = 100% to 100%), 92.9% (95% CI = 80.3% to 100%), and 92.9% (95% CI = 80.3% to 100%), respectively. Two-year locoregional control, progression-free survival, and overall survival for all 19 patients enrolled in study were 94.4% (95% CI = 84.4% to 100%), 89.5% (95% CI = 76.7% to 100%), and 94.7% (95% CI = 85.2% to 100%), respectively ([Supplementary Figure 5](#), available online).

Mean weight loss during therapy among deescalated patients was 4.3% of starting body weight (range = -9.4% to +1.6%). In these patients, no grade 3 acute toxicity during therapy was observed for dermatitis, mucositis, or dysphagia

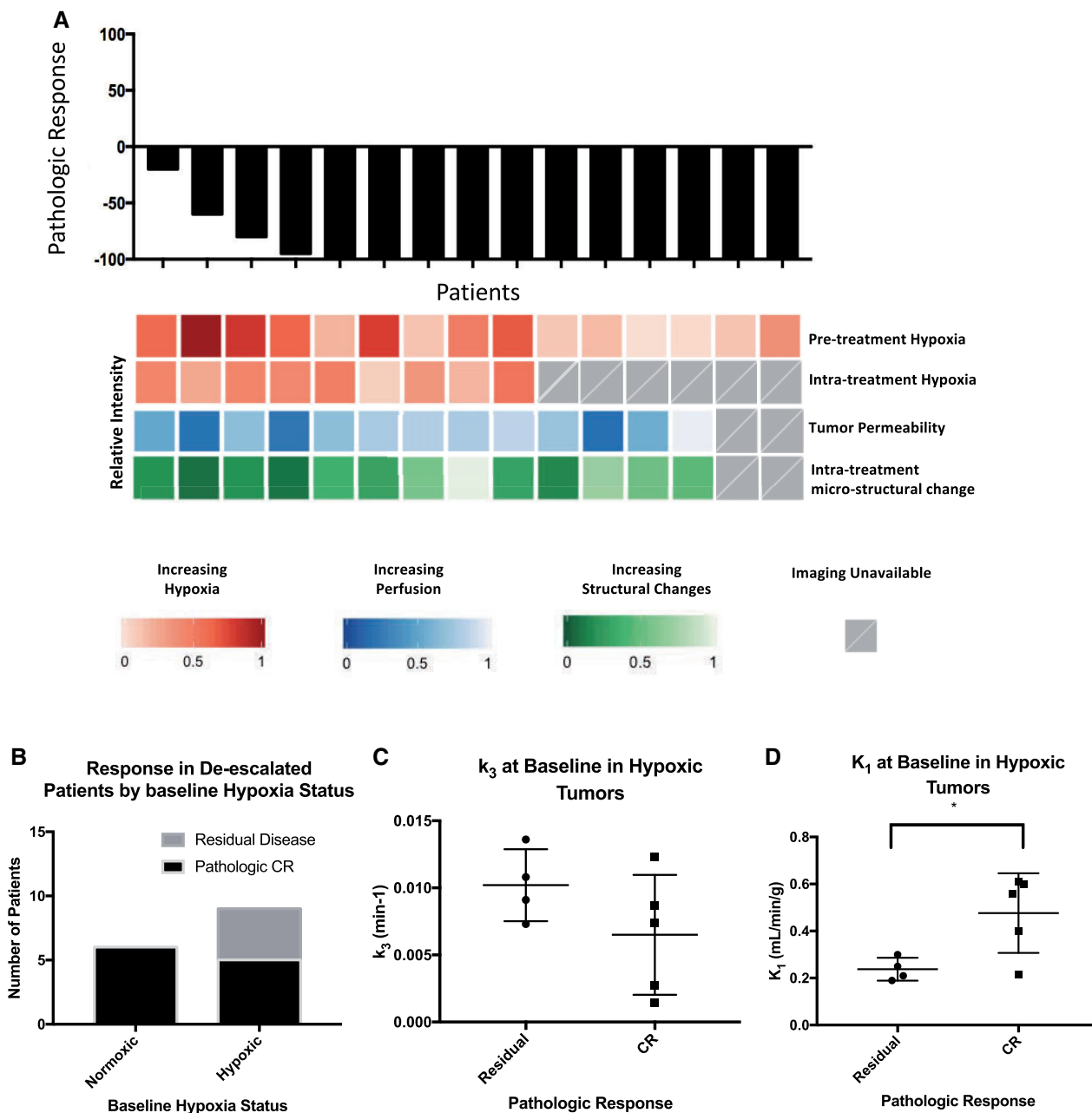


Figure 2. Pathologic results and imaging correlates. **A, top** Pathologic response (percentage of viable tumor, 100%) at the time of neck dissection is shown in 15 patients who received 30Gy. Note that 2 of the 4 patients with residual disease had clinically significant abnormal histologic appearance with unclear viability (see also [Supplementary Figure 4](#), available online). Four of the 19 patients who were not deescalated did not undergo a neck dissection, and all remain without evidence of disease. **Bottom** Compartmental analysis of hypoxia levels (k_3) in cases, pretherapy, and intratherapy is shown (see also [Supplementary Figure 2](#), available online). Note that tumors with no pretherapy hypoxia did not undergo intratherapy scans, and all of these tumors had a pathologic complete response (pCR) (see 2B). Tumor permeability and perfusion (K^{trans} on dynamic contrast enhanced-magnetic resonance imaging [MRI]) was numerically higher in patients with a pCR ($P = .08$; see also [Figure 3A](#)). Relative kurtosis (a surrogate for tumor microstructure on diffusion-weighted-MRI) changed more rapidly in patients with CR in the first week intratreatment ($P = .01$; see also [Figure 3C](#)). **B** Pathologic status by baseline fluorine-18-labeled fluoromisonidazole (^{18}F -FMISO) PET scan. Zero of 6 patients with normoxia at baseline had residual disease at the time of neck dissection compared with 4 of 9 patients with baseline hypoxia ($P = .1$, Fisher's exact test). **C** k_3 values at baseline for patients with pCR tended to be lower, although this was not statistically significant ($P = .11$, t test). **D** For the 9 patients with baseline hypoxia, compartmental analysis revealed a difference in K_1 between those with residual disease and those with complete response ($P = .03$, t test).

([Table 2](#)). No deescalated patient required placement of a feeding tube. Changes in the MD Anderson Dysphagia Inventory (37) and a prospective xerostomia questionnaire (38) (scale = 0-100) increased from baseline by 6.6 and 18.6 points at 4 months, respectively, and by 2.8 and 12.3 points at 2 years, respectively.

On-Therapy Imaging and Circulating HPV-DNA Results

We next sought to determine if functional imaging or circulating viral-DNA could identify pCR at surgery. Compartmental analysis of ^{18}F -FMISO PET scans ([Supplementary Figure 2, B](#) available online) identified that the 4 patients with pathologic

residual disease displayed pretreatment hypoxia and numerically higher levels of hypoxia (k_3) pretreatment (Figure 2, A-C) but also had statistically significantly lower levels of perfusion (K_1 , Figure 2, D). Pretreatment dynamic contrast enhanced-MRI analyses confirmed a difference in perfusion and permeability in patients with residual disease vs those with pCR (Figures 2 and 3, A). Tumor volume on serial MRI demonstrated slow anatomic regression during treatment and did not correlate with pCR (Figure 3, B). Diffusion-weighted-MRI revealed changes in

the apparent diffusion coefficient (a surrogate for tumor cellularity) and relative kurtosis (a surrogate for microstructure) statistically significantly correlated with pCR at time of surgery (Figures 2 and 3, C and D). Circulating viral DNA levels did not correlate with residual disease at neck dissection (Supplementary Figure 6, available online).

Table 2. Radiotherapy-related acute toxicity in deescalated patients (n = 15)^a

Toxicity	CTCAE v4.0 toxicity, No. (%)			
	0	1	2	3-5
Mucositis	5 (33.3)	8 (53.3)	2 (13.3)	0
Dysphagia	4 (26.6)	10 (66.6)	1 (6.6)	0
Dermatitis	3 (20.0)	12 (80.0)	0	0

^aCTCAE = Common Terminology Criteria for Adverse Events.

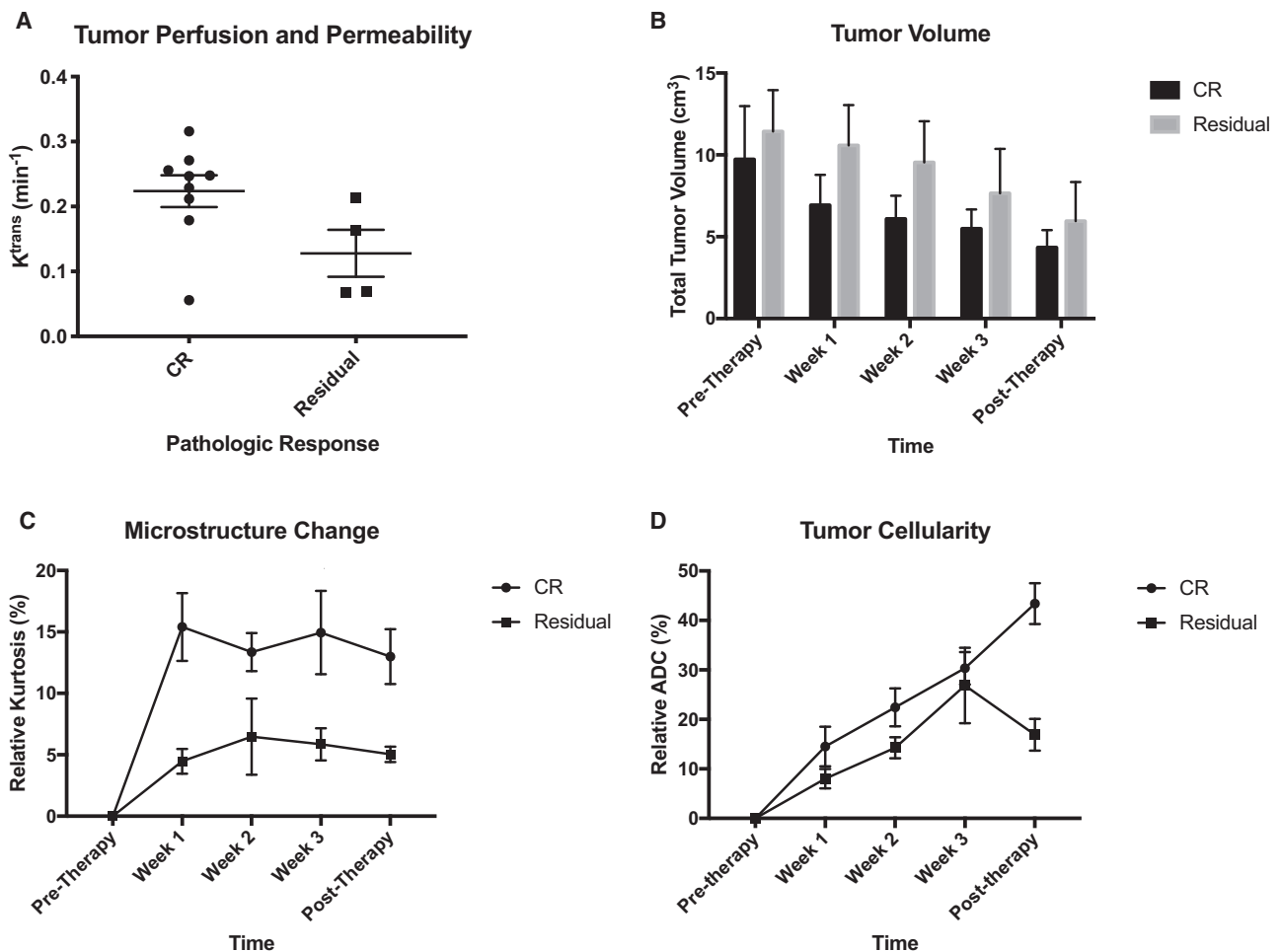


Figure 3. Weekly magnetic resonance imaging (MRI) changes and pathologic response. **A)** Pretreatment dynamic contrast enhanced-MRI-derived quantitative K^{trans} (min⁻¹, a surrogate for tumor perfusion and permeability) demonstrated that K^{trans} is lower in patients with residual disease ($P = .08$; Wilcoxon rank sum test). K^{trans} estimated from a standard Tofts model was incorporated into the shutter speed model. **B)** Tumor volume, determined from T_2 -weighted images, gradually decreased during therapy without a statistically significant difference between those with complete pathologic response and those with residual disease. **C)** Relative kurtosis (a surrogate for tumor microstructure) changed more rapidly in patients with pathologic complete response immediately during therapy and remained different from those with residual disease ($P = .01$, $P = .08$, $P = .03$, and $P = .007$ for week 1, 2, 3, and posttherapy, respectively; all Wilcoxon rank sum test). **D)** Changes in apparent diffusion coefficient (a surrogate for tumor or tissue cellularity) were not statistically significantly different between pathologic response groups until the end of therapy ($P = .17$, $P = .09$, $P = .69$, and $P < .001$ for week 1, 2, 3, and posttherapy, respectively; all Wilcoxon rank sum test).

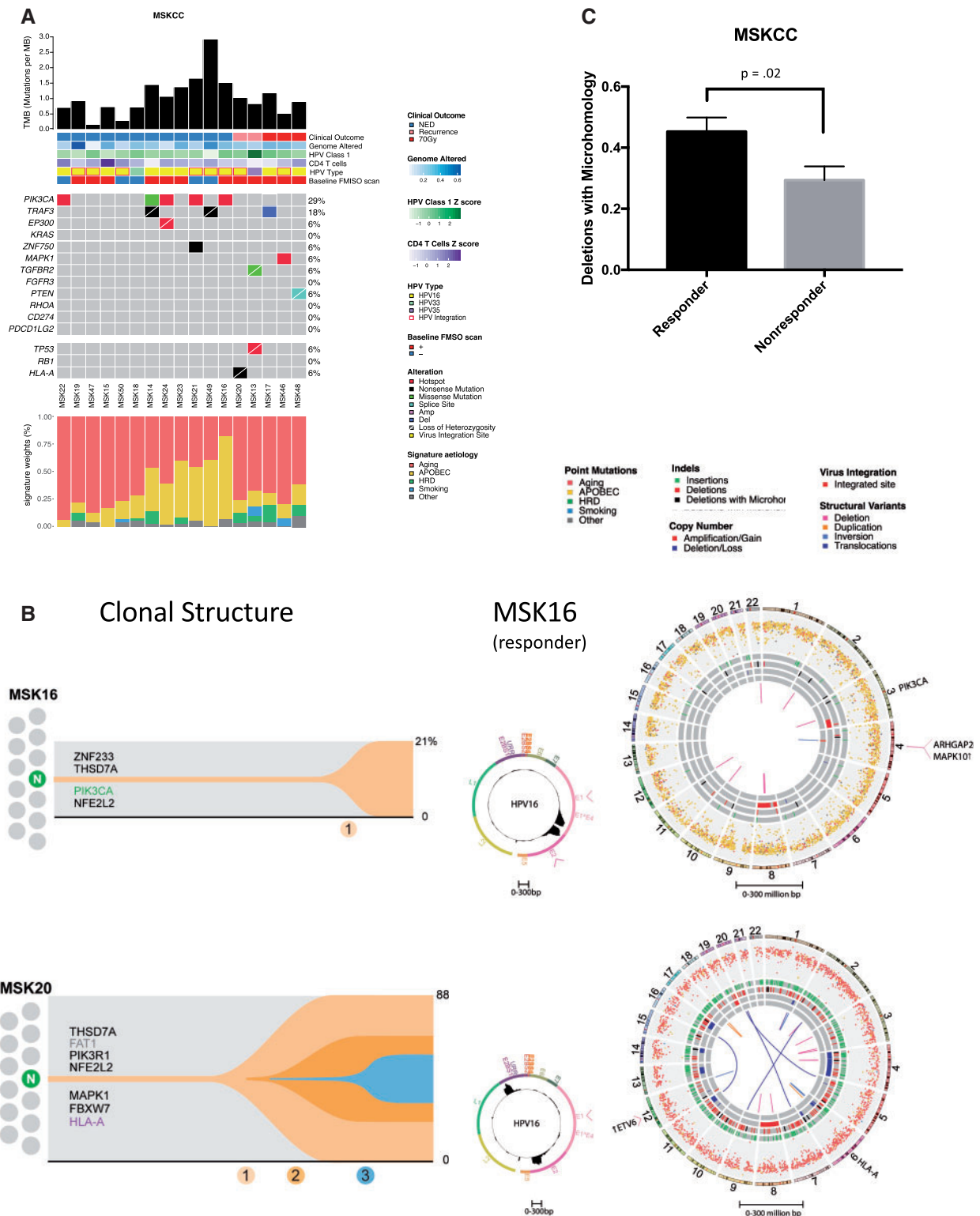


Figure 4. Whole-genome sequencing (WGS) analysis of the Memorial Sloan Kettering Cancer Center (MSKCC) trial. **A** Tumor mutation burden (TMB, mutation/Mb), “genome altered” (percentage of the tumor genome not in a diploid state), genes commonly mutated in human papillomavirus (HPV)-related oropharyngeal cancer, and mutational signatures in the 17 tumor-normal pairs subjected to WGS. CD4 results of T-cell score and HPV Class 1 class are derived from RNA-sequencing analysis. HPV Class 1 class is a single-sample Gene Set Enrichment Analysis of a recently described, poor prognosis, HPV-related expression program (41). HPV subtyping of each case is presented in the annotation bar along with whether the virus is integrated into the host genome. **B** Clonal reconstructions (left) of a responder (MSK16; Figure 4, B [top]) and nonresponder (MSK20; Figure 4, B [bottom]) to low-dose radiotherapy, with clones shown as numbered circular nodes (Supplementary Methods, available online). Circular cells labeled “N” represent the initial normal cell from which the tumor derived, with the x-axis representing increasing accumulation of mutations. The cellular prevalence of each clone is represented by the height of its corresponding polygon. Along the y-axis, with maximal frequency limited by tumor purity. Circos plots (Figure 4, B, right) of both cases demonstrate differences in mutational signatures and structural events (see main text). Tracks are organized from outside to inside according to legend. **C** The proportion of deletions with microhomology is lower among patients who did not respond to low-dose chemoradiotherapy ($P = .02$, Wilcoxon rank sum test).

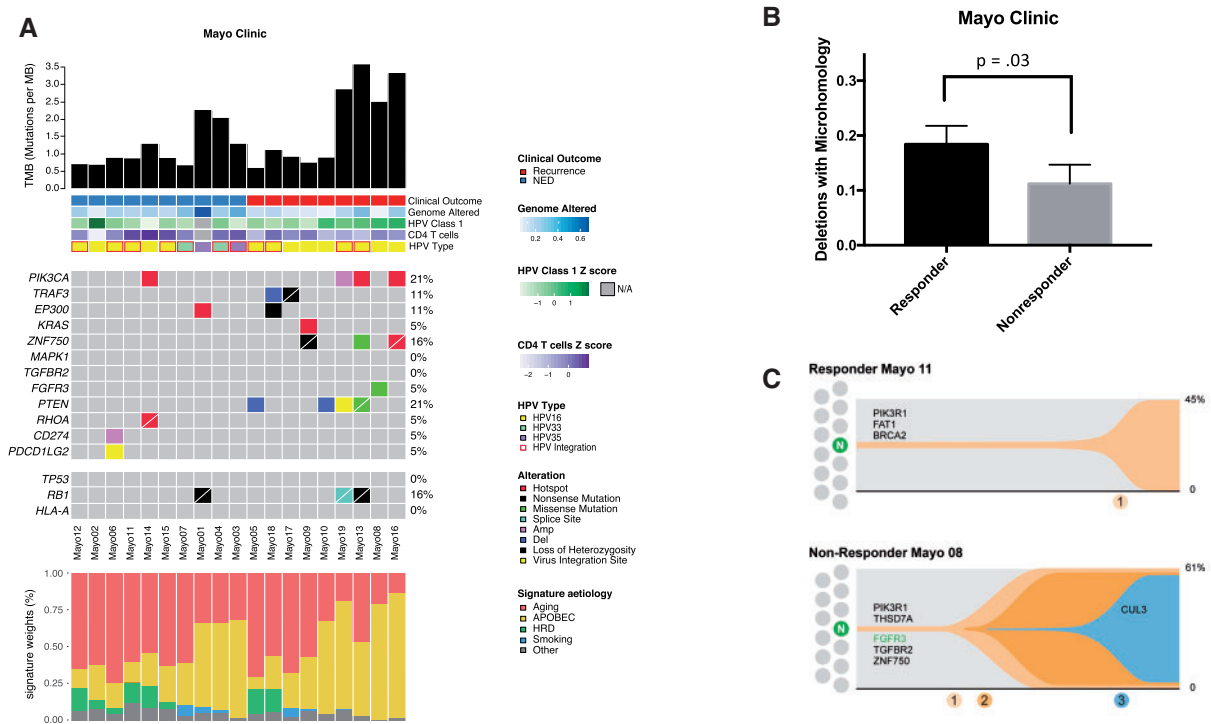


Figure 5. Whole-genome sequencing analysis of the Mayo Clinic cohort. **A**) Mutation burden (mutation/Mb), “genome altered” (percentage of the tumor genome not in a diploid state), genes commonly mutated in human papillomavirus (HPV)-related oropharyngeal cancer, and mutational signatures in the 19 tumor-normal pairs from the Mayo Clinic Cohort. CD4 T-cell score is derived from immune deconvolution of RNA sequencing. HPV subtyping of each case is presented in the annotation bar along with whether the virus is integrated into the host genome. **B**) The proportion of deletions with microhomology is lower in patients who did not respond to low-dose postoperative chemo-radiotherapy ($P = .03$, Wilcoxon rank sum test). NED = no evidence of disease. **C**) Clonal reconstructions of a responding and nonresponding case from Mayo Clinic, with clones shown as numbered circular nodes (Supplementary Materials, available online). Circular cells labeled “N” represent the initial normal cell from which the tumor derived, with the x-axis representing increasing accumulation of mutations. The cellular prevalence of each clone is represented by the height of its corresponding polygon, along the y-axis, with maximal frequency limited by tumor purity.

TRAF3 (18%; Figure 4, A; Supplementary Figure 7, available online; Supplementary Tables 2 and 3, available online). RNA sequencing suggested that responding tumors were more likely to have a productive immune response and less likely to have the previously described HPV Class 1 expression program (41), although neither association was statistically significant (Figure 4, A; Supplementary Figure 7, available online), potentially due to the small sample size. Clonal reconstruction of the tumors analyzed in this study demonstrated that driver mutations were early events in oncogenesis and that nonresponding tumors displayed numerically greater clonal complexity (Figure 4, B; Supplementary Figure 8, available online).

HPV viral replication is facilitated by virus-induced DDR deregulation, which has been posited to mediate the radiosensitivity of HPV-related OPCs (6,18–22). Hence, we used WGS to detect tumors with potential DDR and DSB repair defects and to define whether these may be associated with a favorable response to 30 Gy. WGS revealed that the pattern of single base-substitution mutational signatures was typical of HPV-related malignancies and dominated by aging-related processes and APOBEC-related mutagenesis (Figure 4, A and B) (42). The proportion of small deletions with microhomology, a genomic finding previously reported in HNCs and HPV-related cancers and is indicative of a DSB DNA repair defect (25,42–44), was found to be statistically significantly higher in responding patients than in nonresponding patients ($P = .02$; Figure 4, C).

We next obtained representative tumor material from a cohort of 19 patients from the Mayo Clinic (ClinicalTrials.gov: NCT01932697¹³) who were treated on a deescalation protocol, but in the postoperative setting (30 Gy concurrent with docetaxel). WGS demonstrated that 3 cases harbored RB1 loss-of-function mutations, which are uncommonly found in HPV-related cancers; 2 of these patients developed recurrences (Figure 5, A; Supplementary Figure 10, available online). Consistent with the results of the MSK trial cohort, patients in the Mayo Clinic cohort who responded to 30 Gy displayed a higher proportion of deletions with microhomology than those with recurrence ($P = .03$; Figure 5, B). Patients in the Mayo Clinic cohort who developed recurrent disease also had tumors with more complex clonal structures, less activation of the immune system, and more HPV class 1 expression, although none of these associations was statistically significant (Figure 5, C; Supplementary Figures 9 and 10, C and D, available online).

Discussion

In this pilot study, we have shown that a 60% reduction of radiation to 30 Gy, on the basis of noninvasive, patient-specific ¹⁸F-FMISO PET treatment response using hypoxia as a surrogate for radiosensitivity, is safe and feasible for HPV-related OPC. Using this approach for individualized treatment, we deescalated the

treatment of approximately 80% of HPV-related OPC patients, and no grade 3 radiation-related toxicity was observed. These findings compare favorably with those from a recent deescalation study that reported 40% rates of grade 3 mucositis and dysphagia (12). Further, we anticipate near elimination of the usual long-term treatment-related complications at this low therapeutic dose (45).

Because HPV is known to dysregulate the DDR and DSB repair pathways to facilitate viral integration and replication, we performed WGS to determine whether we could identify a DNA repair defect that may underlie response to 30 Gy. WGS allows for more sophisticated analysis of mutational signature and identified statistically significant differences in deletions with microhomology between patients who responded to 30 Gy and those who did not in both the MSK and May Clinic cohorts. These findings support the notion that response to chemoradiotherapy in patients with HPV-related OPCs may depend on the type of genetic instability and/or DNA repair defects the tumors harbor. Tumor hypoxia has been shown to inhibit homologous recombination DNA repair of DSBs (27,46), and expression of the E7 HPV protein results in downregulation of nonhomologous end-joining by disabling RNF168 (22). Hence, the enrichment in deletions with microhomology identified in HPV-related OPC patients who responded to deescalated radiotherapy analyzed here may have resulted in preferential DSB repair by an error-prone repair pathway, micro-homology-mediated end-joining (22,25).

This study has several limitations. Although we have determined the feasibility of a personalized approach for patients with HPV-positive OPC, because of sample size, the efficacy of the therapeutic strategy described here will require validation in a larger prospective study. Similarly, even though we correlated genomic biomarkers with outcomes in 2 independent studies, the total sample size remains small, and these results will also require validation in larger studies before they can be used clinically. Further, whether 30 Gy of chemo-radiotherapy is sufficient to control disease long term without a neck dissection remains to be determined. Hence, we have initiated a larger phase II study (n=150; ClinicalTrials.gov number, NCT03323463) removing post chemo-radiotherapy neck dissection, which is currently underway. Last, how differences in the 2 concurrent chemotherapy regimens used in the study may affect these results is uncertain and warrants further investigation. Interestingly, another prospective clinical trial (NCT01932697) supports the contention that HPV-related OPC patients can receive markedly reduced doses of radiotherapy, albeit in the postoperative setting (13).

Despite these limitations, the use of biological characteristics of tumors has allowed for a successful deescalation of radiation therapy, laying the foundation as a proof of concept for future studies delivering (chemo)radiation therapy in a biology-driven rather than empiric manner. Our results also provide evidence that a personalized approach, potentially guided by imaging and WGS-based biomarkers, may result in excellent therapeutic response while minimizing debilitating radiation-induced toxicity.

Funding

This work was funded by NIH grant R01 CA157770-01A1, the Serra Family, the James and Judith K. Dimon Foundation, the Imaging and Radiation Sciences Program at MSK, and in part through the National Institutes of Health National

Cancer Institute Cancer Center Support Grants P30 CA008748 and P30 CA016042. JSR-F is funded in part by the Breast Cancer Research Foundation.

Notes

Role of the funders: The funders had no role in the design of the study; the collection, analysis, and interpretation of the data; the writing of the manuscript; and the decision to submit the manuscript for publication.

Disclosures: J.S.R.F. is a consultant of Goldman Sachs, REPARE Therapeutics and Paige.AI, a member of the scientific advisory board of Volition Rx and Paige.AI, and an ad-hoc member of the scientific advisory board of Ventana Medical Systems, Roche Tissue Diagnostics, Genentech, Novartis, and InVivo. N.R. is an ad-hoc consultant for Mirati Therapeutics and REPARE therapeutics, receives research support from Pfizer and BMS, and has received speaker fees from Illumina.

Author contributions: Study conception and design: N.L., N.R., and E.S.; Drafting of manuscript: N.R., N.L., E.S., and J.S.R.F.; MRI analysis: R.P., A.S.-D., N.R., V.H., and N.L.; 18F-FMISO analysis: H.S., M.G., N.L., N.R., and J.H.; Circulating Viral DNA analysis: D.H., N.R., and N.L.; Mutation analysis: X.P., P.S., R.K., N.R., and J.S.R.F.; Clonality analysis: T.N.Y., D.B., P.C.B., N.R., and J.S.R.F.; Indel analysis: X.P., P.S., N.R., and J.S.R.F.; HPV analysis: A.R. and X.P.; RNA analysis: F.K., N.R., and T.A.C.; Study Investigators: N.L., N.R., E.S., N.K., H.S., J.T., J.B., L.G.T.M., S.M., V.H., A.H., D.P., R.J.W., and J.H.; Interpretation of data: all authors; Final approval of manuscript: all authors.

Data Availability

Code to reproduce analysis contained within the manuscript will be made available upon reasonable request. RNA sequencing is available at Gene Expression Omnibus (accession number: GSE157517).

References

- Gillison ML, Koch WM, Capone RB, et al. Evidence for a causal association between human papillomavirus and a subset of head and neck cancers. *J Natl Cancer Inst.* 2000;92(9):709-720.
- Cancer Genome Atlas Network. Comprehensive genomic characterization of head and neck squamous cell carcinomas. *Nature.* 2015;517(7356):576-582.
- Chaturvedi AK, Engels EA, Pfeiffer RM, et al. Human papillomavirus and rising oropharyngeal cancer incidence in the United States. *J Clin Oncol.* 2011;29(32):4294-4301.
- Pfister DG, Ang KK, Brizel DM, et al. National Comprehensive Cancer Network clinical practice guidelines in oncology head and neck cancers. *J Natl Compr Canc Netw.* 2011;9(6):596-650.
- Ang KK, Harris J, Wheeler R, et al. Human papillomavirus and survival of patients with oropharyngeal cancer. *N Engl J Med.* 2010;363(1):24-35.
- Cleary C, Leeman JE, Higginson DS, et al. Biological features of human papillomavirus-related head and neck cancers contributing to improved response. *Clin Oncol (R Coll Radiol).* 2016;28(7):467-474.
- Kimple RJ, Smith MA, Blitzer GC, et al. Enhanced radiation sensitivity in HPV-positive head and neck cancer. *Cancer Res.* 2013;73(15):4791-4800.
- Machtay M, Moughan J, Trotti A, et al. Factors associated with severe late toxicity after concurrent chemoradiation for locally advanced head and neck cancer: an RTOG analysis. *J Clin Oncol.* 2008;26(21):3582-3589.
- Bourhis J, Sire C, Graff P, et al. Concomitant chemoradiotherapy versus acceleration of radiotherapy with or without concomitant chemotherapy in locally advanced head and neck carcinoma (GORTEC 99-02): an open-label phase 3 randomised trial. *Lancet Oncol.* 2012;13(2):145-153.
- Chera BS, Amdur RJ, Tepper J, et al. Phase 2 trial of de-intensified chemoradiation therapy for favorable-risk human papillomavirus-associated oropharyngeal squamous cell carcinoma. *Int J Radiat Oncol Biol Phys.* 2015;93(5):976-985.

11. Mehanna H, Robinson M, Hartley A, et al. Radiotherapy plus cisplatin or cetuximab in low-risk human papillomavirus-positive oropharyngeal cancer (De-ESCALaTE HPV): an open-label randomised controlled phase 3 trial. *Lancet*. 2019;393(10166):51-60.
12. Gillison ML, Trotti AM, Harris J, et al. Radiotherapy plus cetuximab or cisplatin in human papillomavirus-positive oropharyngeal cancer (NRG Oncology RTOG 1016): a randomised, multicentre, non-inferiority trial. *Lancet*. 2019;393(10166):40-50.
13. Ma DJ, Price KA, Moore EJ, et al. Phase II evaluation of aggressive dose de-escalation for adjuvant chemoradiotherapy in human papillomavirus-associated oropharynx squamous cell carcinoma. *J Clin Oncol*. 2019;37(22):1909-1918.
14. Ferris RL, Flamand Y, Weinstein GS, et al. *Transoral Robotic Surgical Resection Followed by Randomization to Low- or Standard-Dose IMRT in Resectable p16+ Locally Advanced Oropharynx Cancer: A Trial of the ECOG-ACRIN Cancer Research Group (E3311)*. Chicago, IL: ASCO; 2020.
15. Bhatia A, Burtress B. Human papillomavirus-associated oropharyngeal cancer: defining risk groups and clinical trials. *J Clin Oncol*. 2015;33(29):3243-3250.
16. Marur S, Li S, Cmelak AJ, et al. E1308: phase II trial of induction chemotherapy followed by reduced-dose radiation and weekly cetuximab in patients with HPV-associated resectable squamous cell carcinoma of the oropharynx-ECOG-ACRIN Cancer Research Group. *J Clin Oncol*. 2017;35(5):490-497.
17. Chen AM, Felix C, Wang PC, et al. Reduced-dose radiotherapy for human papillomavirus-associated squamous-cell carcinoma of the oropharynx: a single-arm, phase 2 study. *Lancet Oncol*. 2017;18(6):803-811.
18. Park JW, Nickel KP, Torres AD, Lee D, Lambert PF, Kimple RJ. Human papillomavirus type 16 E7 oncoprotein causes a delay in repair of DNA damage. *Radiother Oncol*. 2014;113(3):337-344.
19. Rieckmann T, Tribius S, Grob TJ, et al. HNSCC cell lines positive for HPV and p16 possess higher cellular radiosensitivity due to an impaired DSB repair capacity. *Radiother Oncol*. 2013;107(2):242-246.
20. Moody CA, Laimins LA. Human papillomavirus oncoproteins: pathways to transformation. *Nat Rev Cancer*. 2010;10(8):550-560.
21. Cook R, Zoumpoulidou G, Luczynski MT, et al. Direct involvement of retinoblastoma family proteins in DNA repair by non-homologous end-joining. *Cell Rep*. 2015;10(12):2006-2018.
22. Sitz J, Blanchet SA, Gameiro SF, et al. Human papillomavirus E7 oncoprotein targets RNF168 to hijack the host DNA damage response. *Proc Natl Acad Sci USA*. 2019;116(39):19552-19562.
23. Kadaja M, Isok-Paas H, Laos T, Ustav E, Ustav M. Mechanism of genomic instability in cells infected with the high-risk human papillomaviruses. *PLoS Pathog*. 2009;5(4):e1000397.
24. Bristol ML, Das D, Morgan IM. Why human papillomaviruses activate the DNA damage response (DDR) and how cellular and viral replication persists in the presence of DDR signaling. *Viruses*. 2017;9(10):268.
25. Leeman JE, Li Y, Bell A, et al. Human papillomavirus 16 promotes microhomology-mediated end-joining. *Proc Natl Acad Sci USA*. 2019;116(43):21573-21579.
26. Nigro ND, Seydel HG, Considine B, Vaitkevicius VK, Leichman L, Kinzie JJ. Combined preoperative radiation and chemotherapy for squamous cell carcinoma of the anal canal. *Cancer*. 1983;51(10):1826-1829.
27. Bristow RG, Hill RP. Hypoxia and metabolism. Hypoxia, DNA repair and genetic instability. *Nat Rev Cancer*. 2008;8(3):180-192.
28. Swartz JE, Pothen AJ, van Kempen PM, et al. Poor prognosis in human papillomavirus-positive oropharyngeal squamous cell carcinomas that over-express hypoxia inducible factor-1 α . *Head Neck*. 2016;38(9):1338-1346.
29. Brizel DM, Sibley GS, Prosnitz LR, Scher RL, Dewhirst MW. Tumor hypoxia adversely affects the prognosis of carcinoma of the head and neck. *Int J Radiat Oncol Biol Phys*. 1997;38(2):285-289.
30. Evans SM, Koch CJ. Prognostic significance of tumor oxygenation in humans. *Cancer Lett*. 2003;195(1):1-16.
31. Lee N, Schoder H, Beattie B, et al. Strategy of using intratreatment hypoxia imaging to selectively and safely guide radiation dose de-escalation concurrent with chemotherapy for locoregionally advanced human papillomavirus-related oropharyngeal carcinoma. *Int J Radiat Oncol Biol Phys*. 2016;96(1):9-17.
32. Lee N, Nehmeh S, Schoder H, et al. Prospective trial incorporating pre-/mid-treatment [18F]-misonidazole positron emission tomography for head-and-neck cancer patients undergoing concurrent chemoradiotherapy. *Int J Radiat Oncol Biol Phys*. 2009;75(1):101-108.
33. Edge SB, Byrd DR, Compton CC, Fritz AG, Greene FL AT, eds. *AJCC Cancer Staging Handbook: From the AJCC Cancer Staging Manual*. 7th ed. New York, NY: Springer; 2010.
34. Denis F, Garaud P, Bardet E, et al. Final results of the 94-01 French Head and Neck Oncology and Radiotherapy Group randomized trial comparing radiotherapy alone with concomitant radiochemotherapy in advanced-stage oropharynx carcinoma. *J Clin Oncol*. 2004;22(1):69-76.
35. Grkovski M, Lee NY, Schoder H, et al. Monitoring early response to chemoradiotherapy with (18)F-FMISO dynamic PET in head and neck cancer. *Eur J Nucl Med Mol Imaging*. 2017;44(10):1682-1691.
36. Pareja F, Brandes AH, Basili T, et al. Loss-of-function mutations in ATP6AP1 and ATP6AP2 in granular cell tumors. *Nat Commun*. 2018;9(1):3533.
37. Chen AY, Frankowski R, Bishop-Leone J, et al. The development and validation of a dysphagia-specific quality-of-life questionnaire for patients with head and neck cancer: The M. D. Anderson Dysphagia Inventory. *Arch Otolaryngol Head Neck Surg*. 2001;127(7):870-876.
38. Tam M, Riaz N, Kannarunimit D, et al. Sparing bilateral neck level IB in oropharyngeal carcinoma and xerostomia outcomes. *Am J Clin Oncol*. 2015;38:343-347.
39. Gillison ML, Akagi K, Xiao W, et al. Human papillomavirus and the landscape of secondary genetic alterations in oral cancers. *Genome Res*. 2019;29(1):1-17.
40. Agrawal N, Frederick MJ, Pickering CR, et al. Exome sequencing of head and neck squamous cell carcinoma reveals inactivating mutations in NOTCH1. *Science*. 2011;333(6046):1154-1157.
41. Gleber-Netto FO, Rao X, Guo T, et al. Variations in HPV function are associated with survival in squamous cell carcinoma. *JCI Insight*. 2019;4(1):e124762.
42. Alexandrov LB, Nik-Zainal S, Wedge DC, et al. Australian Pancreatic Cancer Genome Initiative. Signatures of mutational processes in human cancer. *Nature*. 2013;500(7463):415-421.
43. Davies H, Glodzik D, Morganella S, et al. HRDetect is a predictor of BRCA1 and BRCA2 deficiency based on mutational signatures. *Nat Med*. 2017;23(4):517-525.
44. Alexandrov LB, Kim J, Haradhvala NJ, et al. The repertoire of mutational signatures in human cancer. *Nature*. 2020;578(7793):94-101.
45. Bentzen SM, Constine LS, Deasy JO, et al. Quantitative Analyses of Normal Tissue Effects in the Clinic (QUANTEC): an introduction to the scientific issues. *Int J Radiat Oncol Biol Phys*. 2010;76(3):S3-S9.
46. Bhandari V, Hoey C, Liu LY, et al. Molecular landmarks of tumor hypoxia across cancer types. *Nat Genet*. 2019;51(2):308-318.